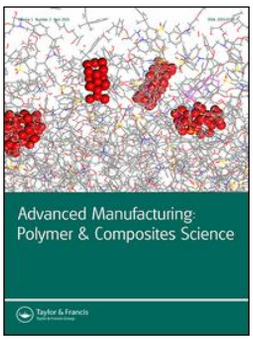

Taylor & Francis
Taylor & Francis Group

Advanced Manufacturing: Polymer & Composites Science

ISSN: 2055-0340 (Print) 2055-0359 (Online) Journal homepage: https://www.tandfonline.com/loi/yadm20

Air evacuation and resin impregnation in semi-pregs: effects of feature dimensions

Sarah G. K. Schechter, Lessa K. Grunenfelder & Steven R. Nutt

To cite this article: Sarah G. K. Schechter, Lessa K. Grunenfelder & Steven R. Nutt (2020) Air evacuation and resin impregnation in semi-pregs: effects of feature dimensions, Advanced Manufacturing: Polymer & Composites Science, 6:2, 101-114, DOI: 10.1080/20550340.2020.1768348

To link to this article: https://doi.org/10.1080/20550340.2020.1768348

Published online: 10 Jun 2020.

ADVANCED MANUFACTURING: POLYMER & COMPOSITES SCIENCE
2020, VOL. 6, NO. 2, 101–114
https://doi.org/10.1080/20550340.2020.1768348

Air evacuation and resin impregnation in semi-pregs: effects of feature dimensions

Sarah G. K. Schechter, Lessa K. Grunenfelder and Steven R. Nutt

Department of Chemical Engineering and Materials Science, University of Southern California, Los Angeles, CA, USA

ABSTRACT

Prepregs with discontinuous resin (semi-pregs) impart robustness to vacuum-bag-only processing of composites. Limited guidance exists for evaluating advantageous resin patterns (i.e. dry space dimensions required to achieve both efficient air evacuation and full resin infiltration during cure). A flow front model was developed based on resin cure kinetics and rheological behavior, and then determined maximum dry space dimensions for semi-pregs under a range of realistic manufacturing conditions. Model predictions were validated *in situ*. Under controlled laboratory cure conditions, small surface openings ($\leq$3.7 mm) resulted in full resin infiltration. Under adverse conditions (resin with accrued out-time), the maximum opening size dropped 40% (to $\leq$2.2 mm). Using a mathematical model, air evacuation time was calculated for various feature sizes using permeability measurements. Model predictions were tested and verified *via* fabrication of laminates. This methodology can be applied to other resin systems to guide vacuum-bag-only prepreg design and support robust production of composites.

KEYWORDS

Prepreg; polymer matrix composites; porosity; defects; carbon fiber; epoxy; out of autoclave processing; vacuum bag only

GRAPHICAL ABSTRACT

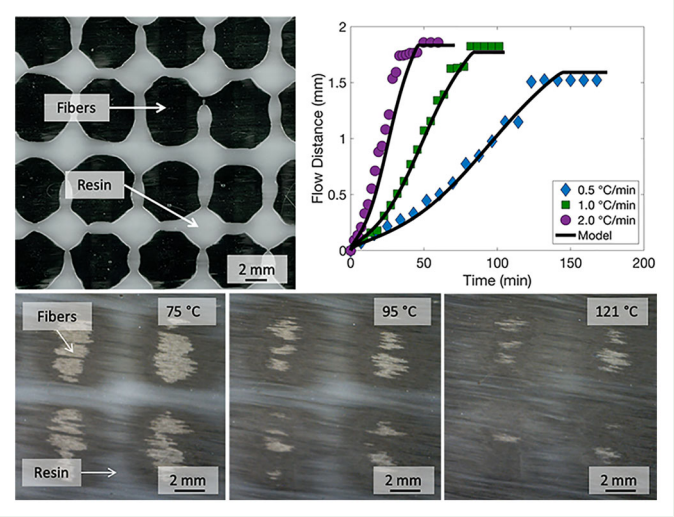

1. Introduction

In this work, we outline a strategy to determine dimensional guidelines for discontinuous resin patterns required to impart robustness to Out-of-Autoclave (OoA)/Vacuum-Bag-Only (VBO) processing of composite prepregs. Currently, aerospace-quality composite materials are cured in autoclaves at pressures of ~5–8 atmospheres. Autoclave pressure suppresses porosity caused by entrapped air, insufficient resin flow, and evolved gases. The autoclave consistently yields parts with low defect content, a quality often referred to as robustness. However, the use of an autoclave has drawbacks, including high capital and operating costs, limited throughput (production bottlenecks), part size restrictions, and high resource use (energy, nitrogen). An appealing alternative is OoA/VBO processing, in which composites are cured in conventional industrial ovens. VBO processing, however, is inherently susceptible to defects from adverse process

CONTACT Sarah G. K. Schechter sarahgka@usc.edu Department of Chemical Engineering and Materials Science, University of Southern California, Los Angeles, CA 90089, USA

conditions, such as poor vacuum, incomplete air evacuation, and/or high humidity. High humidity will increase the moisture content in the resin, which can lead to increased porosity in cured parts [1]. Because at most 0.1 MPa (1 atm) of pressure is exerted on the laminate during VBO processing, air and other gases can remain entrapped during layup and cure. Once the resin gels during the cure cycle, trapped bubbles cannot migrate, resulting in voids and leading to unacceptable porosity levels [2–6]. High defect levels (>1%) diminish mechanical properties and require part rejection. For VBO processing to gain broad acceptance in aerospace, the manufacturing process must yield high quality parts (low porosity) consistently.

Background. Conventional VBO prepregs are fabricated by partially impregnating the fiber bed using a hot-melt process, in which pre-catalyzed resin is formed into a thin film on backing paper and pressed into the fiber bed *via* rollers [2,7]. By design, the resulting prepreg includes dry, highly permeable gas evacuation pathways at the mid-plane of the ply. During manufacturing, using edge-breathing dams and appropriate consumables, these pathways can be sufficient to achieve low defect levels (i.e. porosity) within cured parts [8]. However, in laminates fabricated from conventional VBO prepregs, adverse conditions, such as inadequate vacuum, high levels of absorbed moisture in the resin, or part geometries that prevent in-plane air removal (including large part size), can lead to unacceptable void levels that degrade the mechanical properties of the part [1,9].

VBO prepregs featuring discontinuous resin distributions (i.e. semi-pregs) can potentially limit process-induced defects and impart robustness to the process of manufacturing of aerospace-quality composite materials *via* OoA methods [3–6,10–12]. Grunenfelder et al. [3,11,12] showed that discontinuous resin in prepreg provided air evacuation pathways in the transverse direction, virtually eliminating porosity caused by entrapped air or moisture in OoA/VBO processing. Using this format, cured parts were produced with near-zero internal porosity and no surface defects, even under adverse manufacturing conditions. In contrast, conventional VBO prepreg with continuous resin resulted in unacceptable levels of porosity (3–8%), despite identical process conditions.

The benefit of semi-pregs derives from though-thickness pathways for gas egress, which impart capacity for air evacuation in the *z*-direction (transverse). These pathways can potentially eliminate porosity caused by entrapped gases and low-pressure VBO consolidation. Tavares [10] measured the through-thickness air permeability of a commercially available semi-preg and an equivalent unidirectional prepreg constructed with continuous resin. Results showed that the air permeability of the semi-preg was three orders of magnitude greater than the continuous film prepreg before and during the cure cycle, owing to a network of dry interconnected pore spaces. Discontinuous resin inherently increases the efficiency of evacuating air and, in addition, traps less air at inter-ply interfaces.

While semi-preg formats are commercial products, design and fabrication of such materials has not been thoroughly reported. Previous work by the authors [4,5] focused on developing a technique to create finely tuned resin distribution patterns with varying shapes and sizes that could be applied to a range of reinforcement architectures. The method relied on polymer film dewetting on a low-surface-energy substrate. In this process, resin film was first perforated on backing paper (the substrate) to create an array of nucleation sites. The film was then heated, causing resin to recede (dewet) from the nucleation sites. The resin recession was driven by the surface tension between the low surface energy substrate (the silicone-coated backing paper) and the resin [13–15]. The dewetted resin was transferred onto a fiber bed by pressing the constituents in a hydraulic press. Compared to conventional OoA prepreg formats that feature continuous resin films, prepreg produced using this technique exhibited nearly void-free cured laminates, even when curing under adverse conditions.

Composite part production *via* out-of-autoclave processing requires both efficient air evacuation and full fiber bed infiltration (saturation) with resin. While the use of semi-pregs results in efficient air evacuation, discontinuous resin introduces dry fiber regions and increases resin flow distances. Increased resin flow distances may lead to incomplete fiber bed infiltration and ultimately, porosity. Efficient air evacuation of semi-pregs has been addressed in previous work, but an analysis of *both* efficient air evacuation and subsequent full fiber bed infiltration has not been reported. For example, Tavares [10] developed a 1D resin flow front model to fit results of through-thickness air permeability experiments and predict the air permeability of semi-pregs throughout the cure cycle. The commercial semi-preg analyzed, however, did not achieve full fiber bed infiltration during cure. In a separate study, a geometric model was used to guide semi-preg design for efficient air evacuation [16]. In the present work, we systematically address the design and evaluation of semi-pregs for *both* efficient air evacuation *and* full fiber bed infiltration, considering favorable cure conditions as well as realistic adverse process conditions (i.e. poor vacuum, resin with

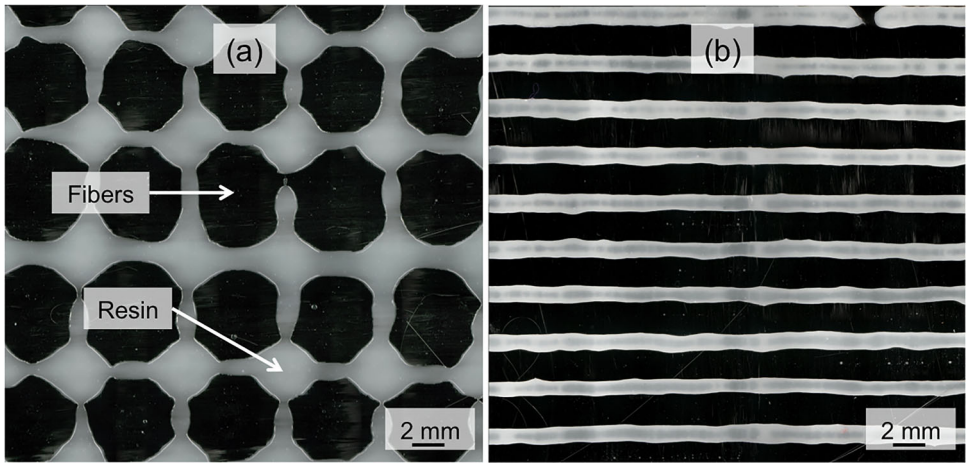

Figure 1. Images show the semi-preg in the initial state (i.e. at room temperature before cure). Both semi-pregs were dewetted for 1 min 30 s at 104 °C and subsequently pressed onto the unidirectional fiber bed using a hydraulic press. (a) Image of the surface of the semi-preg that was fabricated using a spike roller. (b) Image of the surface of the semi-preg that was fabricated using a box cutter.

accrued out-time). Judicious selection of discontinuous resin distribution can mitigate macro-porosity, promote efficient air evacuation from the laminate, and eliminate micro-porosity arising from incomplete fiber wet-out. Additionally, the method presented here can inform future efforts to develop process models required to further expand applications of VBO prepregs.

Objectives. A key challenge to producing composite parts with semi-pregs is ensuring full air evacuation while saturating the fiber bed during the cure cycle. The current work focuses on model-driven design and evaluation of semi-pregs that saturate the fiber bed. While large surface openings maximize air transport, infiltration of large openings requires long lateral flow distances [4,5]. Conversely, smaller surface openings may ensure full fiber bed wet-out because of shorter flow distances. However, small surface openings may be sealed by adjacent prepreg plies if the surface openings do not overlap. Feature size restrictions, moreover, will depend on process parameters, such as ramp rate, dwell temperature, vacuum level, and resin out-time.

The objectives of this work were (1) to define the range of dry space dimensions for a given resin system to ensure complete infiltration while maximizing gas transport, (2) to provide the experimental basis for evaluating this range, and (3) to demonstrate the efficacy of the semi-preg design method in lab-scale laminates. These objectives were motivated by the needs (a) to develop design guidelines for semi-pregs and (b) to increase process robustness in OoA/VBO composite manufacturing.

In the present work, we employ *in situ* observations of prototype semi-pregs to validate a developed model for resin flow fronts, then use the results to inform the design of resin patterns for VBO cure of laminates. A model for resin flow front progression was developed to predict the maximum flow distance under a range of cure conditions. Both favorable and adverse process conditions were analyzed to guide design of appropriate resin pattern dimensions based on representative manufacturing parameters. The adverse cure conditions studied were non-uniform ramp rate, inaccurate dwell temperature, partial vacuum, and resin with accrued out-time. These conditions limit the minimum resin viscosity and flow time achieved during the cure cycle. Semi-preg was produced with dimensions informed by the resin flow model, prototype laminates were fabricated, and the air permeability of the laminates was measured. The results from the *in situ* observations and the prototype laminates corroborate the resin flow front model in the cure conditions tested in this study. These results indicate that the mathematical models used in this study can be used to guide the design of semi-pregs with dry space dimensions required for full tow saturation and efficient air evacuation.

2. Materials & experimental methods

Prepreg fabrication. Following procedures described in previous work [4,5], prepreg samples were fabricated using a unidirectional (UD) carbon fiber reinforcement (Fibre Glast Development Corporation, Ohio, USA) and a toughened epoxy resin (PMT-F4, Patz Materials & Technology, California, USA), which featured medium-to-dry tack. The UD fabric featured an areal weight of 305 grams per square meter (gsm) and a thickness of 0.36 mm. Polyester fill threads were stitched in one direction to hold the UD fibers in place. The tape exhibited negligible crimp, except for the region adjacent to this stitching. The areal weight of resin for all prepreg plies was 76 gsm, yielding prepreg

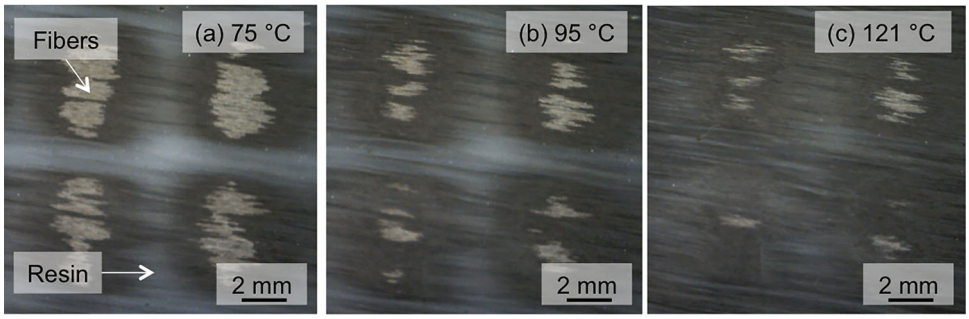

Figure 2. Images of the semi-preg surface on the transparent tool plate during the cure cycle at (a) 75 °C, (b) 95 °C, and (c) 121 °C. The last image shows that the surface opening was still not fully infiltrated by the time the resin underwent gelation.

with a resin content of 33% by weight. The manufacturer's recommended cure cycle for the resin was a ramp of 1.5–3.0 °C per min to 121 °C followed by a two-hour dwell. Prior to this study, the resin was stored in a freezer for approximately 6 months and had accumulated about 7 days of out-life. The material was within specifications, with a recommended storage life of two years at −10 °C, and an out-life of 120 days at room temperature.

Semi-pregs were produced *via* a method of selective dewetting of resin film. With the neat resin film on the silicone-coated backing paper (a low-surface-energy substrate [15]), nucleation sites were introduced using a spike roller (HR-2, Robert A. Main & Sons, Inc., New Jersey, USA) or a box cutter knife. The spike roller pins were spaced at 6.35 mm, and the roller was passed over the entire film in straight passes. Alternatively, a box cutter was used to create evenly spaced resin strips by first scoring parallel lines in the film. The resin film was then placed in an air-circulating oven (Blue M Oven, Thermal Product Solutions, Pennsylvania, USA), to enlarge openings at the nucleation sites. Subsequently, the resin film was attached to the UD fiber bed by pressing the constituents briefly in an unheated hydraulic press (G30H-18-BCX, Wabash MPI). Images of the resultant discontinuous resin pattern on the UD fiber bed using the spike roller or the box cutter are presented in Figure 1(a,b).

Flow front tracking. To monitor the resin flow front during processing, the surfaces of the semi-pregs were tracked *in situ* using the technique described by Hu et al. [17,18]. Four-ply semi-preg stacks (75 mm × 75 mm) were fabricated as described above. The laminates were vacuum-bagged using standard consumables, with the exception of the edge-breathing dams typically required for VBO cure. Edge breathing was eliminated by sealing the perimeter of each laminate with vacuum tape, thus permitting air evacuation only in the through-thickness direction. Each laminate was subjected to a 1-h room-temperature vacuum hold prior to the cure cycle. Resin flow was monitored and recorded during cure using a digital microscope and time-lapse video acquisition (Dino-Lite US, Dunwell Tech, Torrance, CA, USA). Temperature was monitored with a USB thermocouple data logger (Lascar Electronics EasyLog EL-USB-TC-LCD), which was attached adjacent to the laminate and directly on the tool plate. Pressure was tracked using a voltage transducer and data acquisition software (LabVIEW, National Instruments). The maximum pressure of the system was 96.5 kPa (28.5 in Hg). To assess the influence of vacuum level on resin flow during the cure cycle, a regulator was inserted between the vacuum pump and the vacuum bag-assembled laminate, which was adjusted according to the test conditions. To quantify the progression of resin infiltration, images from the recorded video were analyzed. These images were selected from the initial temperature ramp of the cure cycle, at temperatures between 26 and 121 °C with an interval of 5 °C [example images presented in Figure 2(a–c)]. An average diameter of three to six surface openings at each temperature was measured using image-processing software (ImageJ).

Experiments were conducted to evaluate the progression of resin flow front for aged resin during processing. To replicate the increase in degree-of-cure caused by ambient temperature aging (out-time), resin was artificially aged by placing the material in an oven at 85 °C for either 75 min or 109 min. This aging increased the degree of cure, α, to 0.15 and 0.30, respectively. These values were chosen to replicate the values obtained by Kim et al. [19] using a standard industrial epoxy resin system (CYCOM® 5320-1), where $\alpha_0 = 0.15$ corresponds to 28 days of out-time and $\alpha_0 = 0.30$ corresponds to 49 days.

Air permeability measurements. Using results from *in situ* observations, the effective transverse air permeability was measured and compared for the semi-pregs with various dimensions of the surface openings. A custom test fixture was used for the

experiments [20], following the falling pressure method described by Tavares et al. [21]. Plies of prepreg were laid over a cavity of known dimensions supported by stacks of honeycomb core. Measurements were recorded for 4-, 8-, and 16-ply laminates. The edges of the plies were sealed with vacuum tape to allow air evacuation only in the through-thickness direction (no transverse air evacuation). The laminates were covered with consumables (perforated release film and breather cloth), and then vacuum bagged. Vacuum was drawn in the bag to compact the laminate and create a pressure differential between the core cavity and the bag. The evolution of pressure in the cavity was monitored over time using a pressure transducer and data acquisition software, and the measurements were used to estimate an effective air permeability coefficient. All tests were performed at room temperature.

To obtain an average effective air permeability value, two samples (replicates) were tested for each experimental configuration, with a minimum of four pressure decay trials per sample. Each trial was performed until the cavity reached a pressure of 35 kPa, ensuring a uniform level of compaction. Subsequently, the configuration was re-pressurized to begin the next trial. The data from the first trial were omitted because air evacuates more quickly when the consumables and plies have not been previously compressed.

One-dimensional laminar flow of compressible air at isothermal and adiabatic conditions through a porous medium [20] can be described by Darcy's Law:

$$-\frac{KAP_{Bag}}{L\mu V_{Core}}t = \ln\left[\frac{\left(P_{Core}(0)+P_{Bag}\right)\left(P_{Core}(t)-P_{Bag}\right)}{\left(P_{Core}(0)-P_{Bag}\right)\left(P_{Core}(t)+P_{Bag}\right)}\right] \quad (1)$$

where K is the air permeability scalar in the flow direction in m^2, A is the cross-sectional area (1.46×10^{-2} m^2), P_{Bag} is the pressure at the bag side (5×103 Pa), P_{Core} is the pressure at the honeycomb core side in Pa, L is the lateral dimension in m, μ is dynamic viscosity of air (1.85×10^{-5} Pa·s at room temperature), t is time in s, and V_{Core} is the volume of the core (7.87×10^{-4} m^3). The vacuum level was assumed to be 95% (corresponding to an absolute vacuum bag pressure of 5 kPa). Plotting the right-hand side versus time yields a straight-line plot, the slope of which can be used to determine the effective air permeability of the prepreg, K. The honeycomb core was utilized solely as support material and its volume was assumed to be negligible.

Porosity. Finally, using the results from *in situ* observation and air permeability testing, prototype prepregs were fabricated and cured for analysis of part quality. Each prepreg ply was cut to 150 mm × 150 mm. After stacking, the edges of the stack were trimmed, resulting in dimensions of 140 mm × 140 mm. The oven cure cycle was programmed to reach a dwell temperature of 121 °C with a ramp rate of 2 °C/min. For measurements of bulk void content, mutually orthogonal sections were prepared from each laminate center. Cross-sections were polished to 4000 grit on a polishing wheel (LaboPol-2, Struers), and regions 20 mm × 5 mm were examined with a microscope. Images were analyzed using software (ImageJ). A series of manual steps produced a binary porosity image. The void content was calculated from the number of black and white pixels:

$$\text{Porosity} = \frac{p_{black}}{p_{black}+p_{white}} \times 100\% \quad (2)$$

where p is the number of pixels.

3. Resin characterization

Resin cure kinetics model. Following the methodology of Khoun [22] and Kratz [23], modulated differential scanning calorimetry (TA Instruments DSC Q2000) was used to measure the heat flow of resin samples in dynamic and isothermal conditions. Tests were performed under a nitrogen purge at a flow rate of 50 mL/min. For each measurement, 10 ± 2 mg of neat resin was sealed in aluminum hermitic DSC pans (Tzero, TA Instruments). The testing conditions were chosen based on typical process conditions recommended by the manufacturer. To obtain the total heat of reaction of the resin, four ramps were performed at 1, 2, 3, and 5 °C/min from −60 °C to 250 °C, with a temperature modulation of ±0.5 °C/min. Four isothermal dwells were performed at temperatures between 100 °C and 130 °C. Isothermal testing was performed by heating the DSC cell rapidly to the dwell temperature then holding until negligible heat flow was measured. The DSC cell was then cooled to 20 °C, followed by a secondary heating to 250 °C at a constant heating rate of 1.5 °C/min. This final step was performed to measure residual heat of reaction.

Measured heat flow was converted into cure rate using the technique described by Khoun [22]. The DSC heat flow signal was plotted as a function of time, and a linear integration of the area under the heat flow curve was used to calculate the total heat of reaction: 408.5 ± 8.8 J/g for the resin system analyzed here. The degree-of-cure of the resin was obtained by integrating the area under the curve of cure rate versus time. A cure kinetics model was fit to the experimental data, with cure rate described by an autocatalytic model with diffusion factor [24]:

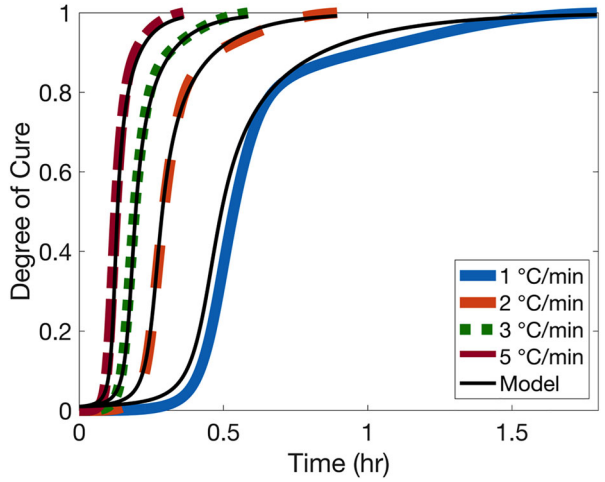

Figure 3. Data measured by DSC for the four dynamic conditions and the predictions obtained with the cure kinetics model.

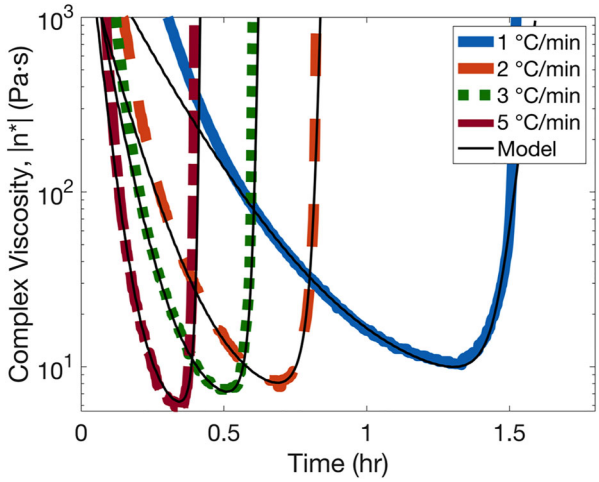

Figure 4. The predicted and measured viscosity evolution with time and temperature.

Table 1. The constants for the resin cure kinetics model that characterizes the resin system PMT-F4A.

Cure kinetics model	
A (s^{-1})	4.86×107
E_a (J/mol)	70,338
m	1.34
n	1.88
C	4.36
α_{C0}	1.15×10^{-7}
α_{CT} (K^{-1})	1.21×10^{-3}

Table 2. The constants for the rheological behavior model that characterizes the resin system PMT-F4A.

Rheological behavior model	
$A_{\mu 1}$ (Pa·s)	7.00×10^{-13}
$A_{\mu 2}$ (Pa·s)	9.54×10^{-2}
$E_{\mu 1}$ (J/mol)	88,822
$E_{\mu 2}$ (J/mol)	12,642
α_{gel}	0.85
A'	0.001
B'	0.001
C'	2.97

$$\frac{d\alpha}{dt} = K\frac{\alpha^m(1-\alpha)^n}{1+\exp\left(C(\alpha-(\alpha_{C0}+\alpha_{CT}T))\right)} \tag{3}$$

where α is the degree-of-cure ($0 \leq \alpha \leq 1$), t is time in s, m and n are reaction exponents, C is a constant, T is temperature in °C, and α_{C0} and α_{CT} (1/K) are fitting parameters. The initial degree-of-cure of the resin was assumed to be 0.005. The rate constant, K, accounts for an Arrhenius temperature dependence:

$$K = A\ \exp\left(\frac{-E_a}{RT}\right) \tag{4}$$

where A is the pre-exponential factor of the cure reaction (1/s), E_a is activation energy (J/mol), and R is the universal gas constant. Figure 3 compares the dynamic DSC data for the four experimental test conditions with the predictions obtained using the kinetics model presented in Equation (3). The numerical values of the model parameters are listed in Table 1. These values were used as a starting point to develop a model for rheological behavior.

Rheological behavior model. Rheology experiments (TA Instruments AR2000) performed on neat resin were used to fit a semi-empirical model for evolution of viscosity [25]. Dynamic scans at heating rates of 2–5 °C/min were performed using a 25 mm parallel plate geometry in oscillatory mode at 0.1% strain and 1 Hz. Resin sample thickness was maintained between 1 and 2 mm. To characterize the rheological behavior of the resin, a model considering the influence of both temperature and the degree-of-cure was implemented. The following equation presents the modified gel model used to describe the evolution of resin viscosity [22,26]:

$$\mu = \mu_1(T) + \mu_2(T)\left(\frac{\alpha_{gel}}{\alpha_{gel}-\alpha}\right)^{(A'+B'\alpha+C'\alpha^2)} \tag{5}$$

$$\mu_i(T) = A_{\mu i}\exp\left(\frac{E_{\mu i}}{RT}\right) \tag{6}$$

where α_{gel} is the degree-of-cure at the gel point and $A_{\mu i}$, $E_{\mu i}$, A', B', and C' are constants. From the temperature-time history measured in each experiment, the degree-of-cure of the resin was calculated using the cure kinetics model and the gel point was determined as $\alpha_{gel} = 0.85$. Equality of the storage and loss shear moduli, G' and G'', was used as a criterion for gelation [27].

After simple manipulation, Equation (5) can be expressed as a linear relationship between viscosity and inverse temperature. Using this approach and data collected prior to the gel point, a linear regression was used to calculate the constants, $A_{\mu 1}$, $E_{\mu 1}$, $A_{\mu 2}$, and $E_{\mu 2}$. The remaining model parameters, A', B', and C', were calculated using a least squares nonlinear regression between viscosity and temperature data. Figure 4 compares the predicted and measured viscosity evolution as a function of time and temperature. The model constants are summarized in Table 2.

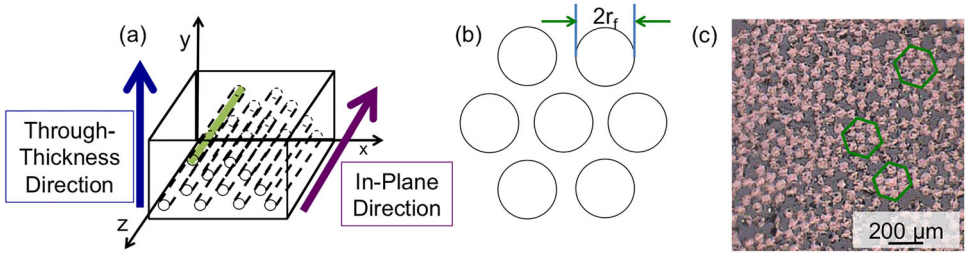

Figure 5. (a) Diagram of the hexagonal arrangement of fibers and labels for the 'through-thickness' and 'in-plane' directions. (b) Diagram of the hexagonal arrangement of fibers and a description of the average fiber radius, r_f. (c) Micrograph of the hexagonal arrangement of fibers.

4. Resin flow model

4.1. Model development

When a stack of prepreg plies is heated, the decrease in resin viscosity accelerates resin flow and impregnation of dry fiber regions. Impregnation continues until either the flow fronts on either side of a dry fiber opening meet, or the degree of cure (and, consequently, viscosity) increases to the point that flow is impeded or arrested. The evolution of the resin flow front was modeled by considering flow of resin within a rigid UD fiber bed [10]. The UD fiber architecture results in intra-tow flow; the inter-tow gaps which lead to dual scale flow in woven fabrics are not present. This intra-tow flow within micron-sized pores yields a saturated flow front [28]. The model development relied on two assumptions: (i) unidirectional flow of the resin (along the fiber direction) only, and (ii) infinite resin supply (flow stops when both fronts meet and not when the initial quantity of resin has been depleted). Utilizing Darcy's law, the advancement of a saturated UD flow front, L, into a rigid fiber bed, under constant applied pressure can be determined as follows [29]:

$$(1 - V_f)\frac{dL}{dt} = -\frac{K_r}{\mu_r}\frac{\Delta P}{L} \tag{7}$$

where μ_r is the resin viscosity (Pa·s) and ΔP is the applied pressure (Pa). For the semi-pregs studied here, the applied pressure was assumed to be equal to the vacuum pressure. The initial degree of impregnation of these semi-pregs was negligible, and thus during initial stages of impregnation, the resin pressure was also assumed equal to the vacuum pressure. This assumption does not hold at high degrees of impregnation, as the fiber bed carries some of the applied pressure. In that case, the applied pressure carried by the resin is less than the vacuum pressure, reducing the pressure that drives the resin into the fiber bed. The fiber volume fraction, V_f, of the prepreg was determined using [30]:

$$V_f = \frac{n \cdot m_f}{Z \cdot \rho_f} \tag{8}$$

where n is the number of plies, m_f is the fiber areal weight (305 g/m^2), Z is the fiber bed thickness (m), and ρ_f is the fiber density (1.75 g/cm^3). Here, the value for V_f was calculated to be 0.6189 (fiber volume fraction of 61.89%). The constant, K_r, is a scalar and represents the permeability of the fabric to the resin in the direction of flow. In the UD fiber bed used in this work, the flow advances primarily along the direction of the fibers within fiber bundles [10]. Resin flow perpendicular to the fibers is negligible, and thus only flow of resin in the fiber direction was studied. Considering a hexagonal arrangement of the fibers (Figure 5), the permeability of the fabric to the resin for the flow parallel to the fiber direction can be calculated using Gebart's formula [31]:

$$K_r = \frac{8r_f^2}{53}\frac{(1 - V_f)^3}{V_f^2} \tag{9}$$

where r_f is the average fiber radius, 5 μm. Here, the calculated value of K_r was 5.45×10^{-13} m^2. For the purpose of modeling simplification, the fiber arrangement was assumed to be hexagonal throughout the structure. While this assumption does not reflect the actual fiber distribution, which will lead to simultaneous micro- and macro-flow, modeling permeability of periodic arrays can provide insights into micro-flow behavior.

The viscosity evolution of the epoxy resin was considered by introducing a function $\mu_r(t)$. In this way, the advancement of the resin flow front, $L(t)$, was modeled considering the cure cycle. Then Equation (7) becomes:

$$\frac{1}{2}L^2(t) = -\frac{K_r}{(1 - V_f)}\Delta P \int_0^t \frac{dt}{\mu_r(t)} \tag{10}$$

The variable, $L(t)$, was measured from the edge of the surface opening to the center of the opening at the point where the resin ceases to flow. The integral of $dt/\mu_r(t)$ was determined from the rheological model characterization of the resin, as discussed in Section 3.

4.2. In situ observation

Conditions can arise during composite cure cycles that alter the viscosity profile of the resin and prevent full resin infiltration, particularly for semi-pregs with large surface openings, including (1) non-

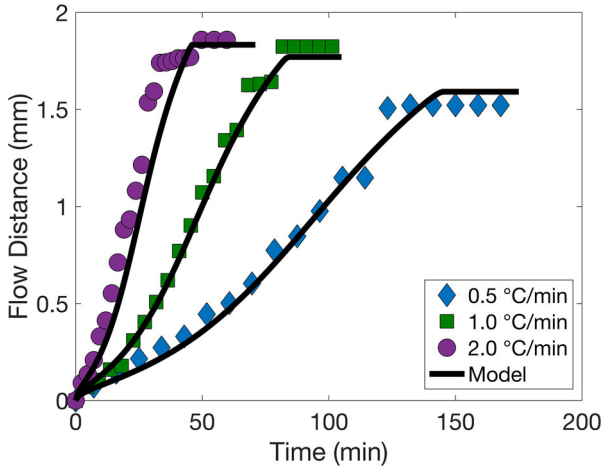

Figure 6. Measured and predicted resin flow distances for favorable cure conditions (uniform ramp rate, accurate dwell temperature, full vacuum, and no aging of the resin) at the three different ramp rates: 0.5, 1.0, and 2.0 °C/min.

uniform ramp rate, (2) inaccurate dwell temperature, (3) partial vacuum, and (4) excessive out-time of resin. Below, achievable resin flow distances were evaluated for each of these adverse conditions during cure. Flow during the one-hour room temperature hold was assumed to be negligible and was not evaluated here.

Favorable cure conditions. Favorable cure conditions consist of a uniform ramp rate, a suitable dwell temperature and time sufficient for resin flow, full vacuum, and resin with minimal out-time. To achieve a uniform ramp rate in this study, the oven was programmed to a temperature above the target temperature. Here, the programmed temperature was 200 °C for a target temperature of 121 °C. Once the laminate reached the target temperature of 121 °C, the oven was quickly reprogrammed to maintain this temperature. The rationale for using a higher set point temperature is described in detail in the next section.

Figure 6 shows measured and predicted resin flow distances for ramp rates of 0.5, 1.0, and 2.0 °C/min. The fastest ramp rate (2.0 °C/min) resulted in the longest resin flow distance – ~1.85 mm, corresponding to a total surface opening diameter of 3.70 mm. In contrast, the slowest ramp rate (0.5 °C/min) yielded the shortest flow distance – ~1.50 mm, or a diameter of 3.00 mm (a difference of 0.70 mm when compared to the value from the fastest ramp rate). The resin flow rates also decreased with decreasing ramp rate (1.11×10^{-2} mm/min for 0.50 °C/min versus 3.99×10^{-2} mm/min for 3.0 °C/min).

Comparing measured and predicted values (Figure 6), the model accurately captured variations in the resin flow front caused by the process conditions selected. Under favorable conditions, the maximum feature size for the resin system studied was 3.8 mm. Additionally, the data showed that a slow ramp rate can result in insufficient resin infiltration, as flow distance decreased with ramp rate.

Non-uniform ramp rate. Normally in composite processing, an oven is programmed to reach a set dwell temperature with a specific ramp rate. However, there is typically a lag, such that the temperature read by the thermocouple in the oven reaches the target dwell temperature before the laminate plies. In practice, the ramp rate measured by a thermocouple within the laminate will decrease as it approaches the dwell temperature.

To explore the influence of this temperature variation on resin flow, the oven cure cycle was programmed to reach a dwell temperature of 121 °C with ramp rates of 0.75, 1.50, or 3.00 °C/min. The resulting flow fronts, both experimental and model predictions, are illustrated in Figure 7(a). At the fastest ramp rate (3.00 °C/min), the measured data match the model predictions. At this higher rate, the ramp rate of the laminate was maintained until the dwell temperature was reached. However, at the slower ramp rates (0.75 and 1.50 °C/min), the measured data did not reach the flow distances predicted by the model due to differences in oven and laminate temperatures. During the 1.50 °C/min ramp, the measured ramp rate shifted to ~0.50 °C/min at 105 °C and remained at this rate until reaching a dwell temperature of 121 °C. The adjusted model prediction in Figure 7(a) includes the ramp rate shift at 105 °C. This decrease in ramp rate also decreased the flow distance, from 1.85 mm to 1.55 mm (or a surface opening diameter of 3.70 mm to 3.10 mm). During the 0.75 °C/min ramp, the rate shifted to ~0.25 °C/min, starting at 80 °C until 121 °C (see the adjusted model prediction in Figure 7(a)). This decrease in ramp rate decreased the flow distance from 1.70 mm to 1.35 mm (or a surface opening diameter of 3.4 mm to 2.7 mm), a difference of 0.35 mm (or 0.7 mm in diameter).

A slower ramp rate led to a larger gap between the desired and actual (non-uniform) ramp rate. This ultimately reduced the resin flow distance. Values for the predicted flow distances for the 1.5 °C/min and 3.0 °C/min ramp rate, interestingly, were both the same as the 1.85 mm (or diameter of 3.70 mm) distance for the 2.0 °C/min ramp rate described in Section 4.2. This result indicates that flow distance did not increase with increasing ramp rate beyond ~1.50 °C/min. Thus, for resin system used here, 3.70 mm was the maximum allowable diameter of a surface opening required to achieve full infiltration.

Inaccurate dwell temperature. In practice, the laminate temperature can differ from the programmed dwell temperature due to inevitable

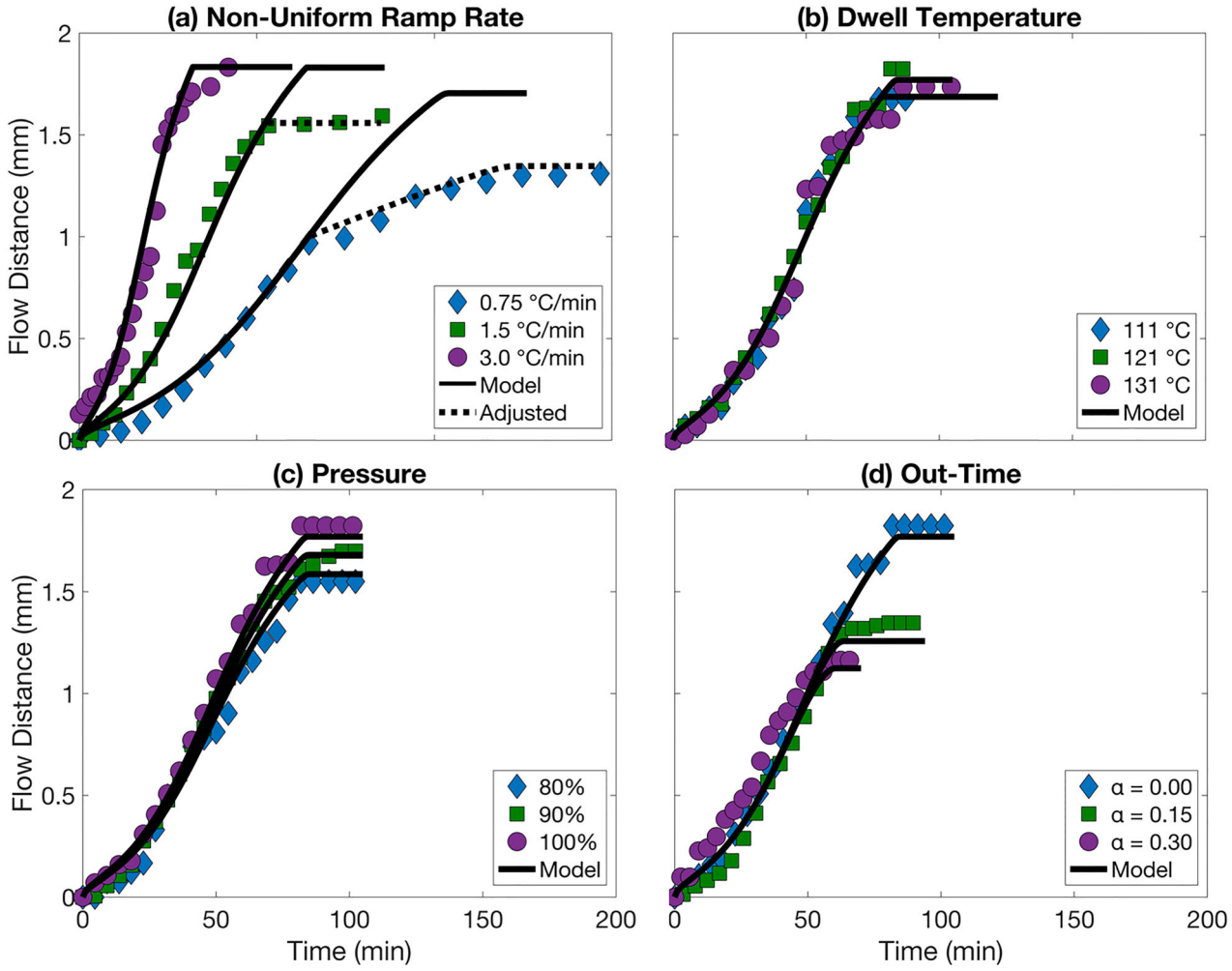

Figure 7. Measured and predicted resin flow distances for: (a) non-uniform ramp rate at 0.75, 1.5, and 3.0 °C/min, (b) inaccurate dwell temperature at 111, 121, and 131 °C, (c) poor vacuum at 80%, 90% and 100% vacuum, and (d) resin that has undergone aging where the degree of cure was 0, 0.15, or 0.30.

thermal gradients, faulty equipment, or location in the oven (i.e. near a vent hole or a heating element). To examine the effect of departures from dwell temperature, a series of experiments were carried out in which the dwell temperature was programmed to be 111 °C, 121 °C, or 131 °C, all achieved *via* a ramp rate of 1 °C/min. The resulting flow distances are presented in Figure 7(b). The maximum flow distance did not differ between 121 °C and 131 °C, at 1.80 mm (or 3.6 mm diameter). A slight decrease in flow distance was observed with a dwell at 111 °C, 1.70 mm (or a surface opening diameter of 3.4 mm). Therefore, the effect of a 10 °C decrease in dwell temperature (reducing flow distance by 0.10 mm) was less than the effects of changes in ramp rate (reducing flow distance up to 0.70 mm), whether under a uniform or non-uniform condition. As with ramp rate, an increase in dwell temperature did not produce additional changes in flow distance above a threshold value (here, 121 °C).

Partial vacuum. In practice, the condition of partial vacuum frequently arises, most often because of bag leaks, and this condition reduces the driving force for resin flow, the difference between atmospheric pressure and bag pressure, or the compaction pressure. In this section, the bag pressure was adjusted to achieve specific levels in relation to the maximum pressure achieved by the pump: 80% (77.2 kPa), 90% (86.9 kPa), and 100% (96.5 kPa). The ramp rate was 1 °C/min, and the dwell temperature was programmed as described above under 'favorable cure conditions'.

The resulting flow distances are presented in Figure 7(c). With each subsequent drop in the vacuum level, a decrease in maximum flow distance and flow rate occurred. At 80% vacuum, the maximum flow distance decreased to 1.60 mm (or 3.4 mm in surface opening diameter), compared to 1.80 mm (or 3.6 mm diameter) at full vacuum. However, the maximum flow distances both occurred at ~84 min, which was due to the decrease in resin flow rate at reduced vacuum. The flow rate for the 80% vacuum condition decreased to 1.89×10^{-2} mm/min, compared to 2.11×10^{-2} mm/min at 100% vacuum. The reduction in vacuum pressure decreased compaction, which ultimately

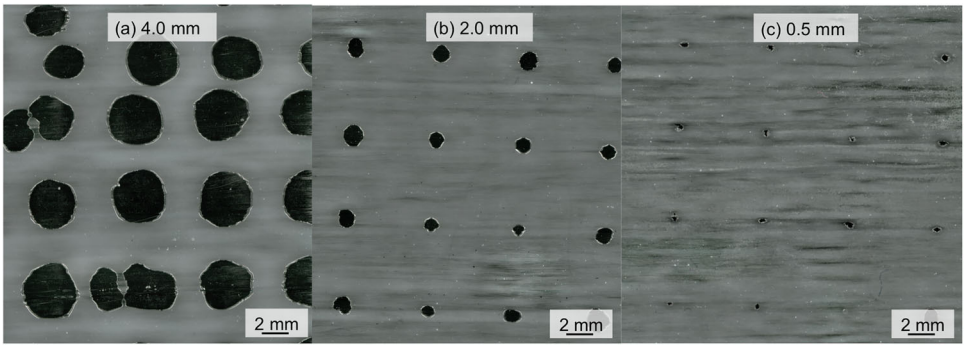

Figure 8. Images of semi-preg produced with film holes of the chosen diameters: (a) 4.0 mm, (b) 2.0 mm, and (c) 0.5 mm.

decreased the resin flow rate. Note that reduced vacuum pressure can also retard or reduce air evacuation from dry regions of prepreg plies, and residual air can prevent resin from infiltrating the fiber bed. Air entrapped in this way, while not accounted for in the flow model, may contribute to the reduced flow distances observed.

Out-time. When resin has accrued minimal out-time, minimum viscosity and maximum flow time generally can be achieved for a given cure cycle, and flow dynamics allow for full wet-out. However, large composite parts can accrue weeks of out-time during lay-up, advancing the degree of cure of the pre-catalyzed resin [19,32–34]. As a consequence, the minimum viscosity increases with out-time, and the amount of time the resin will flow decreases during the heated portion of cure cycle, particularly the first dwell.

The flow distances for different aging periods are shown in Figure 7(d). The rheological behavior model was manipulated by adjusting the initial degree of cure. Here, the laminates underwent a cure cycle of 1 °C/min with a dwell temperature of 121 °C (programmed as described in Section 4.2). For fresh resin (no out-time), the maximum flow distance was 1.75 mm (surface opening diameter of 3.5 mm). At $\alpha_0 = 0.15$, the maximum flow distance decreased to 1.25 mm (surface opening of 2.5 mm), a reduction of 0.50 mm compared to fresh resin. At $\alpha_0 = 0.30$, the maximum flow distance decreased to 1.10 mm (surface opening diameter of 2.20 mm), a reduction of 0.65 mm compared to fresh resin. The reduction in maximum flow distance from fresh resin to $\alpha_0 = 0.30$ was the largest amongst all the adverse process conditions evaluated. Note that the flow rate did not change with an increase in out-time.

5. Room temperature debulk

Design of semi-pregs requires assessment of the efficiency for air evacuation from the laminates. Larger surface openings yield more rapid air evacuation but require longer resin flow distances. In principle, prepreg design must therefore balance the objectives of rapid air evacuation and complete saturation of the fiber bed.

In Section 4, maximum surface opening dimensions were identified for a range of manufacturing conditions. The largest opening diameter (3.7 mm) was associated with a uniform ramp rate of 2 °C/min and represents a judicious balance of the two objectives above. The smallest opening (2.2 mm) was associated with resin aged to $\alpha_o = 0.30$ (equivalent to an out-time of 49 days for CYCOM® 5320-1 [19]), and represents a worst-case scenario in which the two objectives are not balanced.

Permeability measurements of air evacuation in the through-thickness direction were conducted for semi-pregs with the diameters of the two cases described above. In addition, a third diameter, 0.5 mm, was included to understand air evacuation where resin infiltration was not likely to be inadequate. Images of semi-preg with each of the chosen diameters are shown in Figure 8(a–c). The air permeability values obtained from these experiments were used to determine the amount of time required to evacuate 99.99% of air in the laminate, as described below.

Measured air permeability. A summary of the air permeability values of the 4-, 8-, and 16-ply laminates versus surface opening diameter is presented in Table 3. The effective air permeability, K, value decreased with decreasing diameter, as expected. For prepregs with fixed surface opening sizes, air permeability values increased slightly with the number of plies. This finding has implications for fabrication of thick parts, where typically longer room temperature vacuum holds (debulks) are required for prepreg stacks with reduced air permeability (K).

Debulk time. A method typically used to evacuate the air entrapped during the lay-up process of the composite structure is to use debulking, which typically exerts vacuum pressure on the pre-cured lay-up at room temperature. A model for one-dimensional gas transport in composite laminates based on Darcy flow and the ideal gas law is presented below [35–37]. A simple expression for the

Table 3. The average and standard deviation of the effective air permeability, *K*, of laminates made with 4, 8, and 16 plies of semi-preg with surface opening diameters of 0.5, 2.0, and 4.0 mm.

Effective permeability			
Diameter (mm)	Ply count	Sample avg. K (m^2)	Std. dev.
0.5	4	2.34×10^{-17}	5.35×10^{-18}
	8	3.66×10^{-17}	6.97×10^{-18}
	16	7.29×10^{-17}	2.98×10^{-17}
2	4	7.73×10^{-17}	3.38×10^{-17}
	8	2.08×10^{-16}	7.28×10^{-17}
	16	4.18×10^{-16}	1.30×10^{-16}
4	4	9.07×10^{-16}	1.63×10^{-16}
	8	1.56×10^{-15}	3.75×10^{-16}
	16	3.22×10^{-15}	6.81×10^{-16}

mass fraction of gas removed as a function of time and general scaling laws for gas evacuation in laminates was developed. Time, *t*, required to reach a mass fraction of gas remaining in the laminate, m/m_0, as a function of the ratio of the width of the laminate squared, W^2, to the air permeability, *K*, is described as:

$$t = \frac{\mu}{p_0}\frac{W^2}{K}\left[-\frac{1}{0.9}\ln\left(\frac{m}{m_0}\right)\right]^{\frac{1}{0.6}} \tag{11}$$

where μ is dynamic viscosity of air (1.85×10^{-5} Pa·s at room temperature) and p_0 is the initial pressure (here, assumed 95% vacuum or 96×103 Pa).

The time to evacuate 99.99% of air in 4-, 8-, and 16-ply laminates for surface opening diameters between 0.5 and 4.0 mm is presented in Figure 9. The largest surface openings (diameter = 4.0 mm) required only 26 s for evacuation of air from 4 plies of prepreg and 2.5 min for 16 plies. For a diameter of 2.0 mm, the debulk time increased to 5.5 min for 4 plies, and 20.5 min for 16 plies. Finally, for the smallest surface openings (diameter = 0.5 mm), the evacuation time was 18.5 min for 4 plies and 180 min for 16 plies. However, all these times were far less than the time required to debulk prepreg with continuous resin film. The air permeability values of 1-, 2-, 4-, and 8-ply laminates versus fiber surface area exposed were presented previously [4,5]. Using data from that study, the time required to evacuate 99.99% of air from 4 plies or 8 plies of prepreg made with continuous film was 24.5 and 32 h, respectively.

These results indicate that air evacuation was more efficient in semi-pregs with larger dry space dimensions. The debulk time prior to the cure cycle was therefore greatly reduced when using larger surface openings. The trade-off, however, was that overly large dry space dimensions can limit resin infiltration and prevent fiber wet-out during the cure cycle.

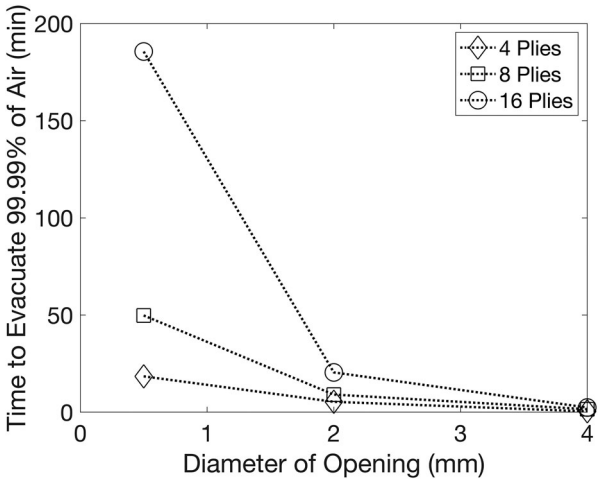

Figure 9. The time to evacuate 99.99% of air in 4-, 8-, and 16-ply laminates for surface opening diameters between 0.5 and 4.0 mm.

6. Experimental validation

Laminates were fabricated from prototype semi-pregs to determine the debulk times required and the internal porosity after cure. The Favorable Cure Conditions (FCC) case (i.e. fast ramp rate, vacuum at highest efficiency, fresh resin, etc.) consisted of an 8-ply laminate made from semi-preg featuring a striped pattern of resin with resin strips of 3.7 mm separated by the same distance. The feature dimensions were determined in Section 4.2, where the maximum dry space distance for full resin infiltration was 3.7 mm for the FCC. Air permeability measurements for this laminate design resulted in a minimum debulk time of slightly less than 2 min to evacuate 99.99% of the air. The Aged Resin (AR) case consisted of the same laminate design as the FCC case, except that the resin was aged to α_o = 0.3. The minimum debulk time was the same for this case. The Adjusted AR case consisted of resin strips separated by 2.2 mm. Feature dimensions were determined using the resin flow front model in Section 4.2 ('out-time'), where the maximum dry space distance for full resin infiltration of resin aged to α_0 = 0.30 was 2.2 mm. Air permeability tests for this laminate design resulted in a minimum debulk time of 2 min 27 s to evacuate 99.99% of the air.

The laminate surface for all three cases resulted in zero porosity (see Figure 10(a–c)). However, for the AR case, evidence of the surface openings was visible as vestiges of the pattern. This pattern indicated local and periodic variations in resin content at the surface, from resin-rich regions (lighter areas) to resin-lean area (darker regions). However, dry exposed fibers (i.e. surface porosity) were not present. Evidence of the surface openings for the FCC case was also present, but the features were much less distinct. For the Adjusted AR case, no surface defects were observed.

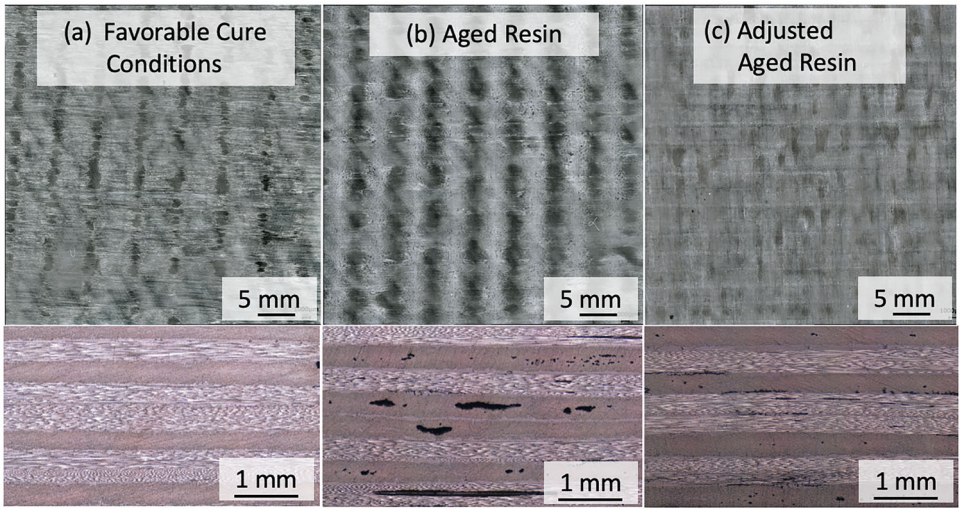

Figure 10. Images of the surface defects and internal void content of the prototype semi-pregs fabricated using the following cases: (a) Favorable Cure Conditions, (b) Aged Resin, and (c) Adjusted Aged Resin.

The three panels showed marked differences in *internal* porosity, however. The FCC case displayed an average void content of 0.1% (Figure 10(a)). On the other hand, the average internal porosity in laminates made from semi-pregs featuring the AR case was 1.6% (Figure 10(b)). The porosity in this case was expected to be much greater than in the FCC case, as the results from this study indicated that aged resin required resin feature spacings that were no more than 2.2 mm. The internal porosity of the Adjusted AR case, designed to account for this prediction, dropped to 0.3%, a decrease of 1.3% from the AR case.

Experimental results described above validated the model predictions using the methodology presented. The debulk time calculated for both the FCC and the Adjusted AR cases were sufficient to fully evacuate air from the laminates. In addition, the dry space dimensions fabricated for both the FCC case and the Adjusted AR case resulted in full fiber bed infiltration, whereas the AR case resulted in insufficient fiber bed wet-out. The results and the methodology described here can be used to guide the design of discontinuous resin patterns for OoA prepregs to ensure both rapid air evacuation and complete resin saturation of fiber beds.

7. Conclusions

A methodology is described for determining the maximum dry space dimensions for semi-pregs produced using a given resin system. While the work focused on a single resin system, the method itself can be applied to any thermoset epoxy. The methodology stems from earlier work [4,5], in which a technique was described for creating discontinuous resin patterns of arbitrary shapes and sizes *via* polymer film dewetting. That technique opened a large design space for prepreg format (semi-preg resin distribution). While earlier work [16] focused on the design and evaluation of semi-pregs based solely on efficient air evacuation, the present work addresses the design of semi-pregs that takes into account the objective of fiber bed saturation.

For the resin studied, a cure cycle was identified that yielded a defect-free microstructure, and surface openings as large as 3.7 mm ensured full fiber bed wet-out. The effects of adverse cure conditions, including inadequate temperature profile, reduced vacuum quality, and resin with accrued out-time, were explored to determine semi-pregs designs to accommodate reduced resin flow distances. In contrast with the favorable cure condition, the maximum surface opening required to ensure full fiber bed wet-out dropped to 2.2 mm for the worst-case scenario (of those considered). The influence of these dry space dimensions on the effective air permeability of the laminates, and ultimately, the time required for evacuation, was determined. The results show that in practice, the design space can be greatly reduced and defined by eliminating patterns that do not allow for (a) full resin infiltration of the fiber bed or (b) sufficient air evacuation.

The model presented provides guidance to specify the dimensions of resin distribution patterns sufficient for both efficient air evacuation and full resin infiltration. However, some aspects of prepreg design were not considered here. First, the evaluation of the resin flow fronts under adverse conditions focused on singular contributions. The *combined* effects of multiple adverse conditions (such as aged resin, non-uniform ramp rate, and poor vacuum quality) will exacerbate the issue, and impede full resin infiltration. Second, only one-dimensional resin infiltration was considered. However, the mechanism for resin infiltration of

more complex fiber beds (particularly woven fabrics) is expected to differ and involve 2D or 3D multi-scale flow. Finally, changing surface opening dimensions ultimately changes the thickness of the resin because of resin recession from nucleation sites during dewetting. Larger surface openings require thicker resin and, ultimately, yield laminates with a larger bulk factor. Prepreg with a large bulk factor can cause laminate wrinkling at part corners and degrade mechanical properties. Understanding how dry space dimensions affect prepreg bulk factor and cured part quality is useful to part fabricators and requires further study. The bulk factor of these resins may be reduced by increasing the degree of impregnation. However, it remains unclear how to incorporate impregnation while retaining the desired pattern. Nonetheless, the method described here is versatile and affords opportunity to design and create discontinuous resin patterns and thus tailor resin distributions to fiber bed features and even part geometry.

The current study can be used to inform the design of VBO semi-preg for virtually any resin system. OoA/VBO prepreg processing presently suffers from a lack of manufacturing robustness, often yielding unacceptable defect levels when conditions are adverse or not adequately controlled. The method described here outlines a pathway to determine favorable (and, eventually, optimal) designs for semi-pregs. Such prepregs can potentially restore robustness to composite manufacturing *via* VBO processing, yielding low defect levels without autoclave pressures. In addition, dewetting is potentially backwards-compatible with hot-melt prepregging, since in principle, imprint/de-wet steps can be incorporated into existing prepreg production lines. The robustness imparted by the methods presented can, in turn, expand applicable uses of VBO prepregs both in aerospace and non-aerospace applications.

Acknowledgements

This project was supported by the M.C. Gill Composites Center. The authors are grateful for material donations from Airtech International (Cole Standish) and to Daniel Zebrine for his assistance.

Disclosure statement

No potential conflict of interest was reported by the authors.

ORCID

Sarah G. K. Schechter http://orcid.org/0000-0001-9000-3093
Lessa K. Grunenfelder http://orcid.org/0000-0001-6561-401X
Steven R. Nutt http://orcid.org/0000-0001-9877-1978

References

[1] Grunenfelder LK, Nutt SR. Void formation in composite prepregs – effect of dissolved moisture. Compos Sci Technol. 2010;70(16):2304–2309.
[2] Jackson K, Crabtree B. Autoclave quality composites tooling for composite from vacuum bag only processing. SAMPE Tech Conf; 2002; Long Beach, CA.
[3] Grunenfelder LK, Dills A, Centea T, et al. Effect of prepreg format on defect control in out-of-autoclave processing. Compos Part A Appl Sci Manuf. 2017;93:88–99.
[4] Schechter SGK, Centea T, Nutt S. Fabrication of out-of-autoclave prepreg with high through- thickness permeability by polymer film dewetting. Sampe Tech Conf.; 2018; Long Beach, CA. p. 2018.
[5] Schechter SGK, Centea T, Nutt SR. Polymer film dewetting for fabrication of out-of-autoclave prepreg with high through-thickness permeability. Compos Part A Appl Sci Manuf. 2018;114:86–96.
[6] Roman M, Howard SJ, Boyd JD. Curable prepregs with surface openings. US 2014/0174641 A1. 2014.
[7] Heth J. From art to science: a prepreg overview. High Perform Compos. 2000;8:32–36.
[8] Repecka L, Boyd J. Vacuum-bag-only-curable prepregs that produce void-free parts. SAMPE Tech Conf; 2002; Long Beach, CA.
[9] Centea T, Hubert P. Modelling the effect of material properties and process parameters on tow impregnation in out-of-autoclave prepregs. Compos Part A Appl Sci Manuf. 2012;43(9):1505–1513.
[10] Tavares SS, Michaud V, Månson J. Assessment of semi-impregnated fabrics in honeycomb sandwich structures. Compos Part A Appl Sci Manuf. 2010; 41(1):8–15.
[11] Grunenfelder LK, Katz S, Centea T, et al. Through-thickness permeable prepreg for robust vacuum bag only processing. SAMPE Tech Conf; 2017; Seattle.
[12] Nutt S, Grunenfelder L, Centea T. High permeability composite prepreg constructions and methods for making the same. PCT/US2018/012665; 2018.
[13] Kheshgi HS, Scriven LE. Dewetting: nucleation and growth of dry regions. Chem Eng Sci. 1991; 46(2):519–526.
[14] Roy S, Bandyopadhyay D, Karim A, et al. Interplay of substrate surface energy and nanoparticle concentration in suppressing polymer thin film dewetting. Macromolecules. 2015;48(2): 373–382.
[15] Kohl JG, Singer IL. Pull-off behavior of epoxy bonded to silicone duplex coatings. Prog Org Coat. 1999;36(1-2):15–20.
[16] Schechter SGK, Centea T, Nutt S. Effects of resin distribution patterns on through-thickness air removal in vacuum-bag-only prepregs. Compos Part A Appl Sci Manuf. 2020;130: 105723.
[17] Hu W, Grunenfelder LK, Nutt SR. In-situ observation of void transport during vacuum bag-only cure. SAMPE Tech Conf; 2016; Long Beach, CA.

[18] Hu W, Grunenfelder LK, Centea T, et al. In-situ monitoring of void evolution in unidirectional prepreg. J Compos Mater. 2017;21:2847–2858.
[19] Kim D, Centea T, Nutt SR. Modelling and monitoring of out-time and moisture absorption effects on cure kinetics and viscosity for an out-of-autoclave (OoA) prepreg. Compos Sci Technol. 2017; 138:201–208.
[20] Kratz J, Hubert P. Anisotropic air permeability in out-of-autoclave prepregs: effect on honeycomb panel evacuation prior to cure. Compos Part A Appl Sci Manuf. 2013;49:179–191.
[21] Tavares SS, Michaud V, Månson J. Through thickness air permeability of prepregs during cure. Compos Part A Appl Sci Manuf. 2009;40(10): 1587–1596.
[22] Khoun L, Centea T, Hubert P. Characterization methodology of thermoset resins for the processing of composite materials – case study. J Compos Mater. 2010;44(11):1397–1415.
[23] Kratz J, Hsiao K, Fernlund G, et al. Thermal models for MTM45-1 and Cycom 5320 out-of-autoclave prepreg resins. J Compos Mater. 2013;47(3): 341–352.
[24] Hubert P, Johnston A, Poursartip A, et al. Cure kinetics and viscosity models for Hexcel 8552 epoxy resin. Int SAMPE Symp Exhib. 2001;46: 8552.
[25] Halley PJ, Mackay ME. Chemorheology of thermosets – an overview. Polym Eng Sci. 1996;36.
[26] Castro JM, Macosko CW. Kinetics and rheology of typical polyurethane reaction injection molding systems. Soc Plast Eng. 1980:434–438.
[27] Mezger TG. The rheology handbook: for users of rotational and oscillatory rheometers. 2nd ed. Hannover: Vincentz Networks; 2006.
[28] Carlone P, Palazzo GS. Unsaturated and saturated flow front tracking in liquid composite molding processes using dielectric sensors. Appl Compos Mater. 2015;22(5):543–557.
[29] Michaud V, Mortensen A. Infiltration processing of fibrereinforced composites: governing phenomena. Compos Part A Appl Sci Manuf. 2001;32: 981–996.
[30] Gay D. Composite materials: design and applications. 3rd ed. Boca Raton: CRC Press, Taylor & Francis Group; 2015.
[31] Gebart BR. Permeability of unidirectional reinforcements for RTM. J Compos Mater. 1992;26(8): 1100–1133.
[32] Grunenfelder LK, Nutt SR. Out time effects on VBO prepreg and laminate properties. Proc SAMPE 2011 Conf, Long Beach, California; 2011.
[33] Centea T, Kratz J, Hubert P. The effect of out-time and cure cycle on the consolidation of out-of-autoclave prepregs. Proc. 11th Int. Conf. Flow Process. Compos. Mater., Auckland, New Zealand; 2012.
[34] Grunenfelder LK, Centea T, Hubert P, et al. Effect of room-temperature out-time on tow impregnation in an out-of-autoclave prepreg. Compos Part A Appl Sci Manuf. 2013;45:119–126.
[35] Arafath ARA, Fernlund G, Poursartip A. Gas transport in prepregs: model and permeability experiments. Proc 17th Int Conf Compos Mater, Edinburgh, United Kingdom; 2009, p. 1–9.
[36] Helmus R, Centea T, Hubert P, et al. Out-of-autoclave prepreg consolidation: coupled air evacuation and prepreg impregnation modeling. J Compos Mater. 2016;50(10):1403–1413.
[37] Centea T, Nutt SR. Manufacturing cost relationships for vacuum bag-only prepreg processing. J Compos Mater. 2016;50(17):2305–2321.